

## X-ray tomography analysis of bubbles and slugs in a fluidized bed with inter-particle force

Ma, Jiliang; Liu, Daoyin; Chen, Xiaoping; Liang, Cai; van Ommen, J. Ruud

**DOI**

[10.1016/j.ijmultiphaseflow.2021.103835](https://doi.org/10.1016/j.ijmultiphaseflow.2021.103835)

**Publication date**

2021

**Document Version**

Final published version

**Published in**

International Journal of Multiphase Flow

**Citation (APA)**

Ma, J., Liu, D., Chen, X., Liang, C., & van Ommen, J. R. (2021). X-ray tomography analysis of bubbles and slugs in a fluidized bed with inter-particle force. *International Journal of Multiphase Flow*, 145, Article 103835. <https://doi.org/10.1016/j.ijmultiphaseflow.2021.103835>

**Important note**

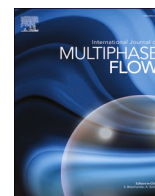
To cite this publication, please use the final published version (if applicable). Please check the document version above.

**Copyright**

Other than for strictly personal use, it is not permitted to download, forward or distribute the text or part of it, without the consent of the author(s) and/or copyright holder(s), unless the work is under an open content license such as Creative Commons.

**Takedown policy**

Please contact us and provide details if you believe this document breaches copyrights. We will remove access to the work immediately and investigate your claim.



# X-ray tomography analysis of bubbles and slugs in a fluidized bed with inter-particle force

Jiliang Ma<sup>a,\*</sup>, Daoyin Liu<sup>a</sup>, Xiaoping Chen<sup>a</sup>, Cai Liang<sup>a</sup>, J. Ruud van Ommen<sup>b</sup>

<sup>a</sup> Key Laboratory of Energy Thermal Conversion and Control of Ministry of Education, School of Energy and Environment, Southeast University, Sipailou No.2, 210096, Nanjing, China

<sup>b</sup> Department of Chemical Engineering, Delft University of Technology, Van der Maasweg 9, 2629HZ, Delft, the Netherlands

## ARTICLE INFO

### Keywords:

Fluidized bed  
Inter-particle force  
X-ray tomography  
Bubble  
Slug

## ABSTRACT

Bubbles and slugs coexist in a fluidized bed with strong inter-particle forces. However, the effects bubbles and slugs impose over fluidizing stability, and chemical reaction efficiency are different. The present work distinguished bubbles and slugs with the aid of X-ray tomography, and the evolution of their properties with varying inter-particle force in a fluidized bed were studied. The results show that the gas-holding capacity of the emulsion phase improves as inter-particle forces initially increase. In this process, the bubble frequency decreases noticeably, and the bubble size slightly increases. Bubbles rise slower than theoretically predicted because inter-particle force reduces the particle flow. The frequency and the size of slugs increase with inter-particle forces. As forces initially increases, the slug size increases with measurement height. An opposite trend is observed when inter-particle forces continues to strengthen. Near the gas distributor, the slug rising velocity is independent of size. In contrast, large slugs have a higher velocity than small slugs near the bed surface. Finally, three slugging patterns are distinguished, and the influence they impose on particle flow is analyzed.

## 1. Introduction

Gas-solid fluidization with inter-particle attractive forces (hereafter referred to as inter-particle force) is common in industrial processes (Lin et al., 2020). The inter-particle force attenuates the kinetic energy of particles upon collision (Wang et al., 2016), changing the fluidization dynamics, sometimes causing the fluidization process to fail (Zhou et al., 2017; LaMarche et al., 2017). Therefore, it is necessary to obtain deeper insight into the relationship between fluidization dynamics and inter-particle force.

As the inter-particle force initially increases, the emulsion phase is prone to maintaining a stable structure (Shabanian and Chaouki, 2017), causing the fluidization characteristics of Geldart group B particles to behave as group A (Seville and Clift, 1984; McLaughlin and Rhodes, 2001; Wormsbecker and Pugsley, 2008). Extensive studies have been conducted, focused on minimum fluidization (Escudero and Heindel, 2013; Makkawi and Wright, 2004), fluidization regime (Xu et al., 2014), and particle flows (Xu et al., 2015; Zhou et al., 2016; Boyce et al., 2017). When the inter-particle force further increases, particles may adhere together, forming agglomerates (Shabanian and Chaouki, 2016; Liu

et al., 2017). If the force is strong enough to maintain a continuous growth of agglomerates, partial or total defluidization occurs (Gomez-Hernandez et al., 2016; Bartels et al., 2008).

Bubbles are typical in fluidized beds; they can reverse the agglomeration process by breaking the agglomerates via shear stress (Parveen et al., 2013; Weber et al., 2011). Bubbles also play an important role in particle mixing, heat, mass transfer, and the conversion of gaseous reactants (Kohler et al., 2020; van der Schaaf et al., 2002). Therefore, bubbling behaviors in a fluidized bed with inter-particle force have attracted attention.

The effects of inter-particle force on the size, frequency and rising velocity of bubbles have been studied (Shabanian and Chaouki, 2015; Shabanian and Chaouki, 2016; Ma et al., 2016; Shabanian and Chaouki, 2014). It was reported that the bubble size decreases as the inter-particle force initially increases, because the gas tends to pass through the gap between particles rather than allowing the formation of individual bubbles (Shabanian and Chaouki, 2015). As the force further increases, bubble sizes begin to increase because the force facilitates the coalescence of bubbles (Shabanian and Chaouki, 2016; Ma et al., 2016). Our previous work on bubble behaviors found that fluidization fails in a way

\* Corresponding author.

E-mail addresses: [jlma@seu.edu.cn](mailto:jlma@seu.edu.cn) (J. Ma), [dylu@seu.edu.cn](mailto:dylu@seu.edu.cn) (D. Liu), [xpchen@seu.edu.cn](mailto:xpchen@seu.edu.cn) (X. Chen), [liangc@seu.edu.cn](mailto:liangc@seu.edu.cn) (C. Liang), [J.R.vanOmmen@tudelft.nl](mailto:J.R.vanOmmen@tudelft.nl) (J.R. van Ommen).

<https://doi.org/10.1016/j.ijmultiphaseflow.2021.103835>

Received 21 May 2021; Received in revised form 14 July 2021; Accepted 20 September 2021

Available online 22 September 2021

0301-9322/© 2021 Elsevier Ltd. All rights reserved.

of alternation between normal fluidization and whole-bed slugging when the inter-particle force is strong enough by X-ray tomography (Ma et al., 2019a). Notably, the voids detected by X-ray tomography involved bubbles and slugs, individually affecting the fluidizing dynamics. Therefore, it is necessary to distinguish slugs from bubbles and investigate their respective behaviors with varying inter-particle force.

The present work uses X-ray tomography to capture the “voids” in a bubbling column and distinguished them as bubbles and slugs. The effects of inter-particle force on the properties of bubbles and slugs at different measurement heights are discussed. Furthermore, the relationship between the rising velocity and the equivalent diameter of bubbles and slugs is analyzed. Finally, slugging patterns under strong inter-particle force are also provided.

## 2. Experimental description

### 2.1. Material preparation

The inter-particle force was introduced by coating inert particles with a polymer layer where cohesiveness depends linearly on temperature (Shabaniyan et al., 2013). The coating process was performed in a rotary drum. A mixed solution of Poly ethyl acrylate (PEA) and poly methyl methacrylate (PMMA) (commercial name, Eudragit NE30D). It was sprayed onto rolling particles. At the same time, a stream of high-temperature air was injected into the drum to evaporate the water in the coating solution, resulting in the solidified polymer layer. The coating solution was sprayed in several batches to keep the polymer layer the same thickness throughout. Between batches, sufficient time was provided for the liquid to evenly distribute over all particles. By adjusting the total volume of solution and the number of particles in the drum, the polymer layer thickness was controlled to about 10  $\mu\text{m}$ . Furthermore, the polymer layer was very thin relative to particle diameter; thus, the influence of the polymer layer thickness on particle size can be neglected. Table 1 lists the properties of the bed materials.

### 2.2. Experimental setup

Fig. 1 shows a schematic of the experimental setup. The fluidized bed was made of Perspex with an inner diameter of 0.14 m and a height of 1.6 m. Air was used as the fluidizing medium. The fluidization gas velocity,  $U_g$ , was kept at  $2.5U_{mf}$  for all cases. The particle temperature changed from 25°C to 45°C by adjusting the temperature of the fluidizing medium. Bouffard et al. proposed equations to predict the inter-particle force between two coated particles and were used to estimate the inter-particle force in this work (Bouffard et al., 2012). As the temperature increased from 25°C to 45°C, the inter-particle force increased linearly from 2.5 to 6 times the particle gravity. Because prediction errors for these equations may be present, bed temperature was used to qualitatively represent the inter-particle force in the following figures. The influence of temperature on air properties was neglected because the experiment was performed near ambient temperature, and the variance in air properties was too small to affect the fluidization dynamics.

The “voids” in the bed (bubbles and slugs) were detected by a multi-source X-ray tomography system built at TU Delft. The measurement

**Table 1**  
Property of bed materials.

Item	Value	unit
base particle	glass beads	-
Diameter	600	$\mu\text{m}$
Density	2500	$\text{kg}/\text{m}^3$
minimum fluidization velocity of uncoated particles, $U_{mf}$	0.325	$\text{Nm}/\text{s}$
polymer layer	PEA/PMMA	-
layer thickness	10	$\mu\text{m}$

principle of X-ray tomography can be described by the Beer–Lambert law (Lau et al., 2018):

$$I = I_0 e^{-\mu x} \quad (1)$$

where  $I_0$  and  $I$  are the intensity of X-ray lines before and after passing through a slab of material with thickness  $x$ ,  $\mu$  is the attenuation coefficient that depends on the property of materials. X-ray tomography is commonly used to detect bubbles in fluidized beds (Lau et al., 2018; Maurer et al., 2015a; Maurer et al., 2015b). When scanning a fluidized bed with a fan beam of X-rays, the solid length that each X-ray line travels through can be calculated by measuring  $I$  and  $I_0$ . In the present work, three X-ray sources were placed at 120° around the column. Each source generated a fan-beam X-ray whose intensity was measured by a detector array across the column. The output data of detectors was recorded for 1 minute at a sampling frequency of 2500 Hz. Detailed parameters of the system can be found in the reference (Ma et al., 2019a).

### 2.3. Data processing

#### 2.3.1. Calibration

The purpose of the calibration was to build a functional relationship between the output of each detector and the solid length each X-ray line passes through. A seven-point calibration was performed to reduce the influences from beam hardening from the X-ray source tubes, (Mudde, 2011). By scanning an empty bed, a full bed and a partially filled bed, we plotted a curve through the seven calibration points using the following equation based on the Beer–Lambert law:

$$I = A + B \exp(-x/C) \quad (2)$$

where  $A$ ,  $B$  and  $C$  are the calibration coefficients,  $x$  is the calculated solid length, and  $I$  is the detector output. Since the calibration coefficients largely depend on the nature of the source tubes and detectors, all 192 detectors and three tubes had to be calibrated separately. Detailed information about the calibration process can be found in Ma et al., (2019).

#### 2.3.2. Reconstruction

The bed cross section was then discretized by a grid of  $50 \times 50$  pixels. The solid length set was converted to the void fraction in each pixel using an iterative reconstruction algorithm that combines the simultaneous algebraic reconstruction technique (SART) and modified one step late (OSL) method (Mudde, 2010).

#### 2.3.3. Binarization

The void fraction appeared as gray levels; therefore, the reconstructed image had to be binarized. The threshold value was determined using pipes of known dimensions. A cylindrical pipe with an internal diameter of 52 mm was inserted vertically in a packed bed. By adjusting the threshold values applied to the reconstructed gray-scale image, the optimal threshold value was determined if the binary image provided the best area reproduction of the pipe. From this, a threshold value of 0.68 was gained for this work. The raw and the binary images are shown in Fig. 2.

#### 2.3.4. Stacking

By stacking the binary images on top of each other for all consecutive points, quasi-3D versions of bubbles passing through the measurement plane were obtained, as shown in Fig. 3. The vertical axis is time (s), and the horizontal axis is the column dimension (mm). The minimum bubble size, that can be detected by the setup, is a diameter of about 2 cm, if this is the only bubble presenting in the cross-section at that time. If multiple bubbles are present, larger bubbles will cast a ‘shadow’ over smaller ones, making them difficult to detect (Brouwer et al., 2012).

Fig. 4 shows the schematic for estimating the rising velocity of voids

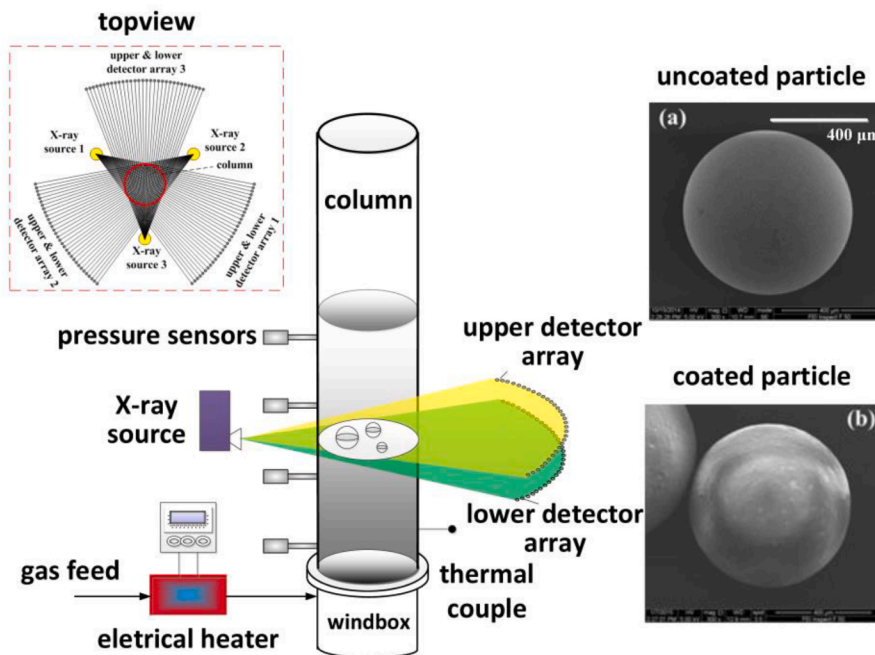


Fig. 1. Schematic of experimental setup.

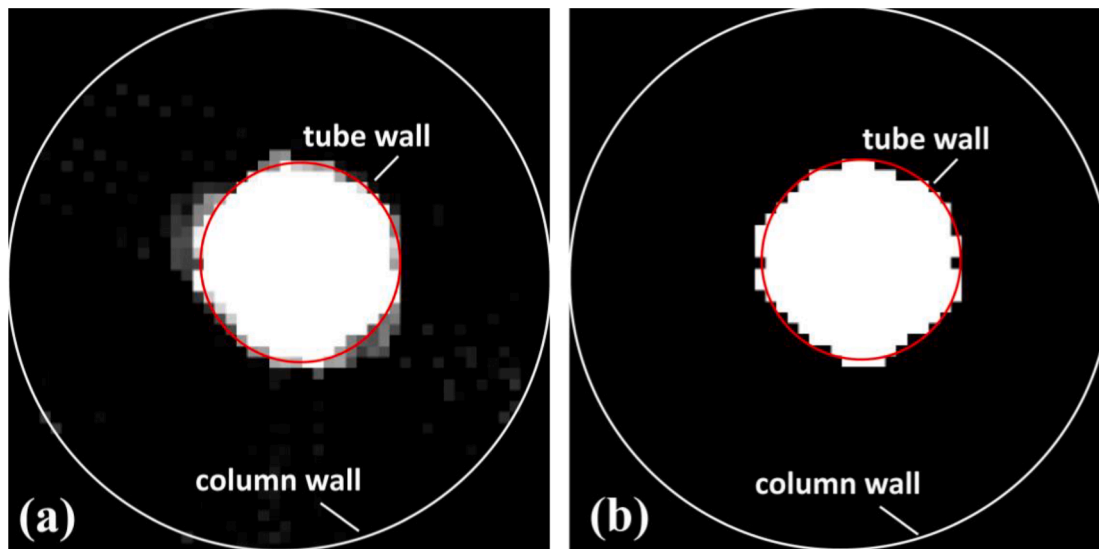


Fig. 2. Reconstructed image of a cylindrical pipe inserted in a packed bed. (a) raw image; (b) binary image.

in the bed. It was estimated as the ratio of the distance between lower and upper planes to the time difference for the center of gravity of each void passing through both planes. Since the distance between two measurement planes in the bed center was 1.09 cm, the void rising velocity  $U_v$  was calculated as  $U_v=0.0109/\Delta t$ .

### 3. Results and discussions

#### 3.1. 3D version of reconstructed voids

Fig. 5 illustrates the 3D temporal images of reconstructed voids passing through the cross-section at heights of 70 mm and 230 mm under different inter-particle forces. As indicated in Fig. 5(a), the voids in the vicinity of the gas distributor are sensitive to the inter-particle force. Under a mild force, most voids are small and inter-locked as multi-structured voids (Azizpour et al., 2012). The void frequency

decreases, whereas the size increases with increasing inter-particle force. When the force is strong enough, the projection diameter of voids approaches to the bed diameter. At this time, the entire bed was pushed upward in a process called “whole-bed slugging”. The voids continued growing via coalescence with the elevation of measurement height at a given inter-particle force. Unexpectedly, this behavior is not observed for strong inter-particle force. The voids at 230 mm are not as large as those observed at lower planes (Fig. 5(b)). This phenomenon may be attributed to the disintegration of slugs before reaching elevated heights. Therefore, smaller voids were observed at higher heights.

The voids captured by X-ray tomography include bubbles and slugs. Slugging is usually regarded as a consequence of continuous bubble growth, but the dynamics of bubbles and slugs and their influence on particle flow are different. Therefore, it is meaningful to distinguish bubbles and slugs and extract their respective properties. Fig. 6 shows a schematic for distinguishing bubbles and slugs. The first step is to

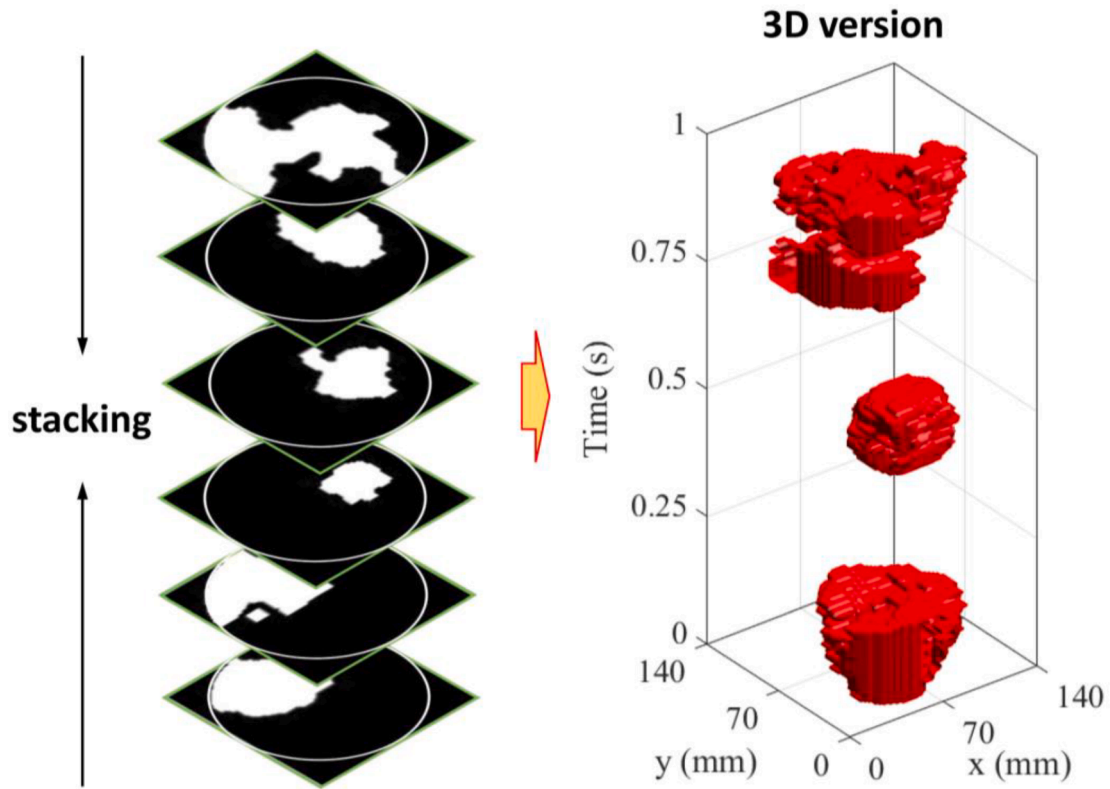


Fig. 3. 3D version of bubbles obtained by stacking reconstructed images.

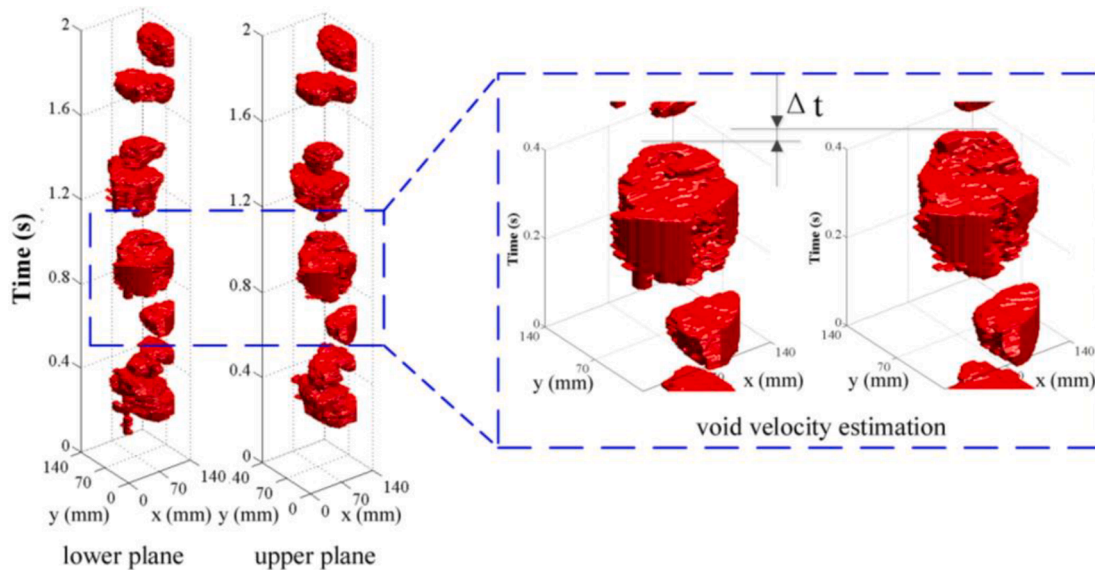


Fig. 4. Determination of void rising velocity.

determine the smallest cube encompassing the void. Next, the average of length and width of the cube  $(x+y)/2$  is compared with  $\lambda D$ , where  $D$  is the column diameter and  $\lambda$  is the threshold coefficient. The void is identified as a slug when  $(x+y)/2$  is larger than  $\lambda D$ ; otherwise, it is regarded as a bubble.

The threshold coefficient  $\lambda$  is critical for distinguishing slugs from bubbles. We changed  $\lambda$  from 0.85 to 1 and plotted the number of identified slugs, shown in Fig. 7. As seen, the number of slugs changes around 45 when  $\lambda$  increases from 0.85 to 0.99. Beyond 0.99, the number of slugs sharply drops to zero. Because the slug is the void occupying the cross-

section of the column, we chose 0.99 as the threshold coefficient. The reason that the threshold coefficient  $\neq 1$  may be due to reconstruction errors and the difference between the discretized grids and the actual column.

### 3.2. Properties of bubbles and slugs

#### 3.2.1. Cross-sectional hold-up

Fig. 8 shows the cross-sectional hold-up of bubbles and slugs at different measurement heights and inter-particle forces. The

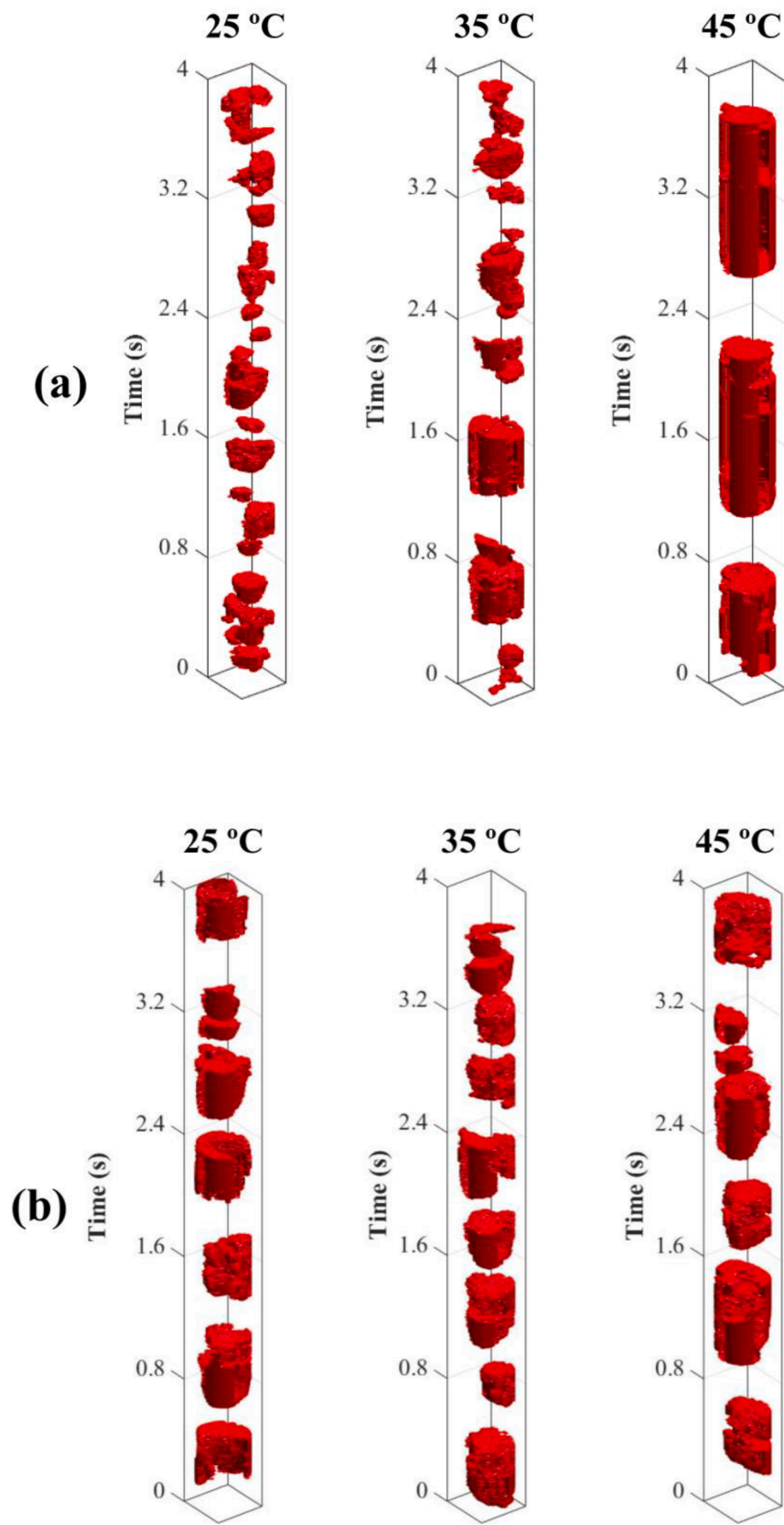


Fig. 5. 3D temporal images of reconstructed voids at different measurement heights and inter-particle force. (a) height: 70 mm, (b) height: 230 mm.

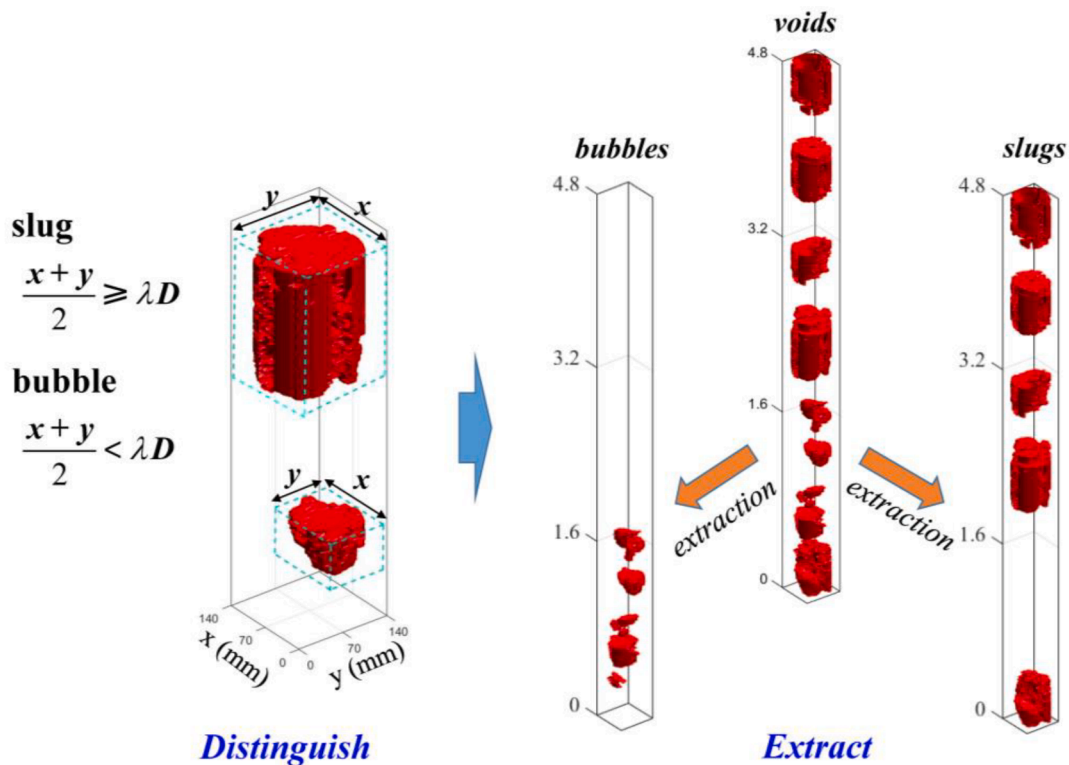


Fig. 6. Schematic for distinguishing bubbles and slugs from reconstructed voids.

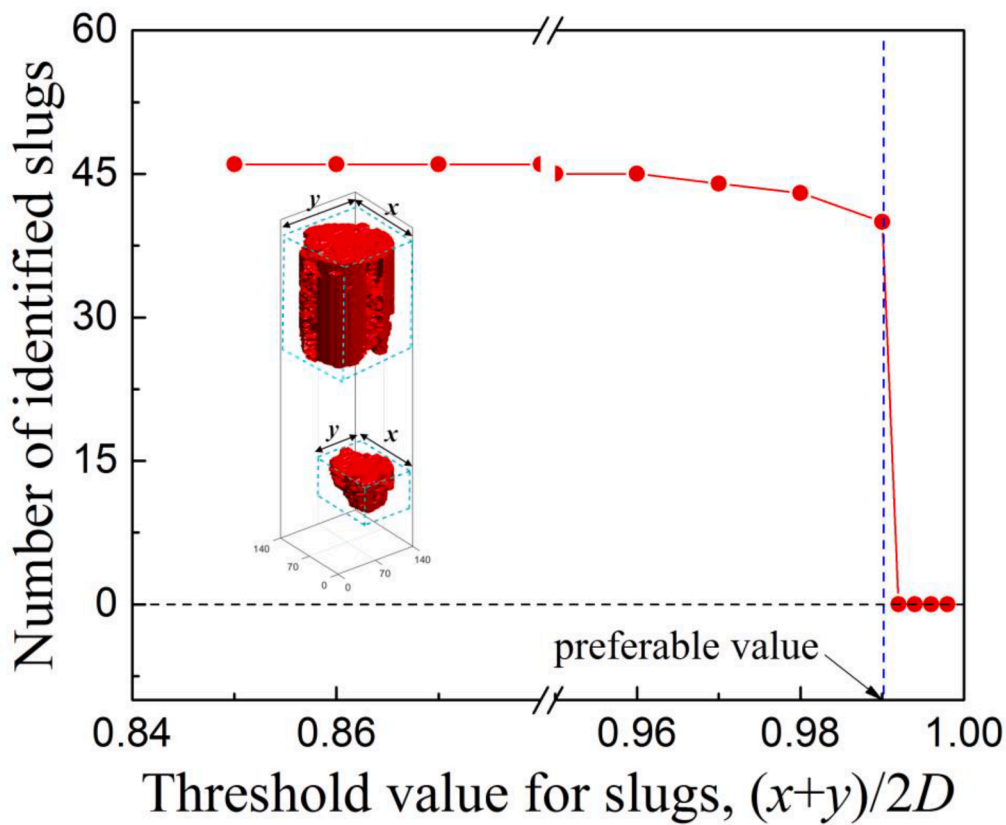


Fig. 7. Sensitivity of identified slugs to threshold coefficient

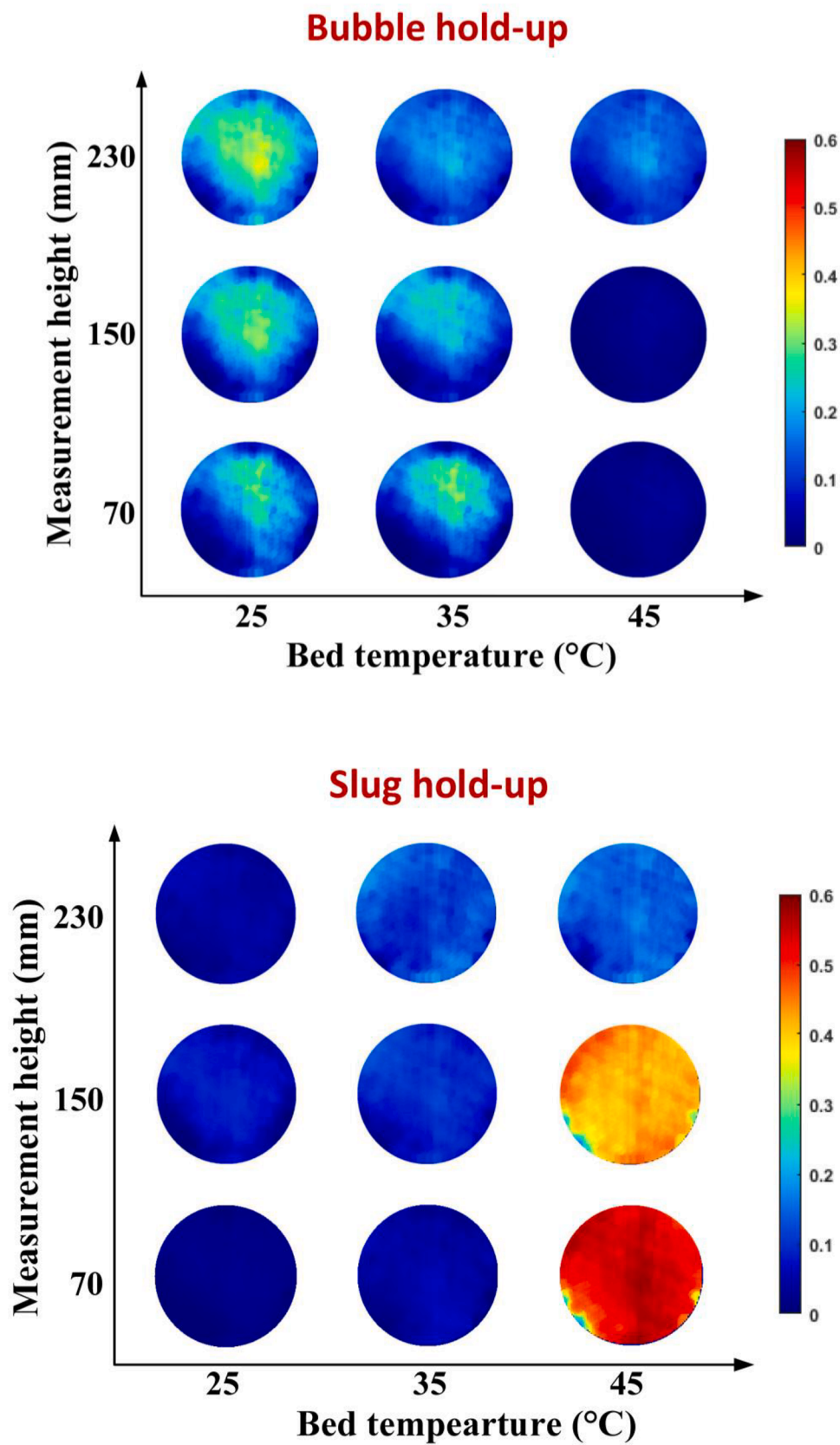


Fig. 8. Hold-up of bubbles and slugs at different measurement heights and inter-particle force.

measurement heights are 70 mm, 150 mm and 230 mm. Under a mild inter-particle force, the hold-up of bubbles increases with the measurement height due to bubble growth. For the medium-cohesive case, the bubble hold-up decreases with the measurement height, implying that the bubbles have grown to a size similar to the bed dimensions, becoming slugs. When the force is strong enough, the bed was dominated by whole-bed slugging. Thus, the bubble hold-up at 70 mm and 150 mm is close to zero. At a given height, the bubble hold-up gradually decreases with increasing inter-particle force.

The hold-up of slugs is close to zero for the case of mild inter-particle force because the bubbles dominated the bed. As the force increases, slugs appear, and their hold-up increases with the measurement height. When whole-bed slugging occurs at the strongest inter-particle force, the slugs rise from the distributor and ruptures in the rising process. Therefore, fewer slugs are detected at higher heights, and the slug hold-up decreases with measurement height.

### 3.2.2. Frequency

Fig. 9 plots the effects of inter-particle force on the frequency of bubbles and slugs detected at different heights. With the elevation of measurement height, the bubble frequency decreases whereas the slug frequency increases. This is because bubbles grow via coalescence with the rising process. At the same time, large bubbles are prone to trigger slugging. When the bed temperature increases from 25 °C to 30 °C, the bubble frequency at 150 mm and 230 mm decreases slightly and sharply at the height of 70 mm. The decrease indicates that the bubbles near the distributor are more sensitive to the inter-particle force. When the bed temperature exceeds 35 °C, the bubble frequency at all heights decreases sharply and converges around a similar value close to zero. As the inter-particle force increases, the slug frequency visibly increases while the differences among various heights gradually diminishes. When the inter-particle force is strong enough, the frequency of slugs is close to 1 Hz, and the bed is dominated by whole-bed slugging.

### 3.2.3. Equivalent diameter

Fig. 10 shows the variation in the equivalent diameter of bubbles and slugs with the inter-particle force and measurement height. The equivalent diameter is the diameter of sphere with the same volume to the reconstructed bubble/slug. Only a slight increase in bubble diameter was observed as the inter-particle force increases. This occurrence indicates that the growth of bubbles with the inter-particle force may be not attributable to bubble coalescence. As shown in Fig. 9, the bubble frequency decreases with the inter-particle force. It can be inferred that the excess gas passes through the interstitial gap between particles instead of presenting as bubbles. In other words, the bed has a higher capacity for holding gas in its emulsion phase. Similar results were also reported by Shabanian and Chaouki (2014). The diameter of slugs also increases slightly when the bed temperature ranges from 25 °C to 35 °C. Beyond 35 °C, the slug diameter at different heights shows different sensitivities to the inter-particle force. A sharp increase in slug diameter was observed at a 70 mm measurement height. The slug diameter at 230 mm height shows little dependence on the inter-particle force. The appearance of whole-bed slugging is the main reason for this abnormal trend. The slugging starts at the gas distributor and passes by the measurement planes sequentially without raining down any particles. These slugs may rupture in the rising process, resulting in less whole-bed slugging being detected at higher heights. Therefore, as the temperature increases beyond 35 °C, a sudden jump of slug diameter is observed at 70 mm height, whereas only a slight change is found at 230 mm height. Notably, the diameter of some slugs is larger than the column diameter (0.14 m), because the slugs are large in length, making their equivalent volume diameter larger than the column diameter.

As discussed previously, the behaviors of bubbles and slugs near the distributor are sensitive to the inter-particle force. The size distributions of bubbles and slugs in the vicinity of the distributor under different inter-particle forces are plotted in Fig. 11. The size distribution was also fitted using a Gamma function because it gives the best fit for the case without inter-particle force (Rüdisüli et al., 2012a). As seen, the bubble size distribution moves to the right side as the inter-particle force

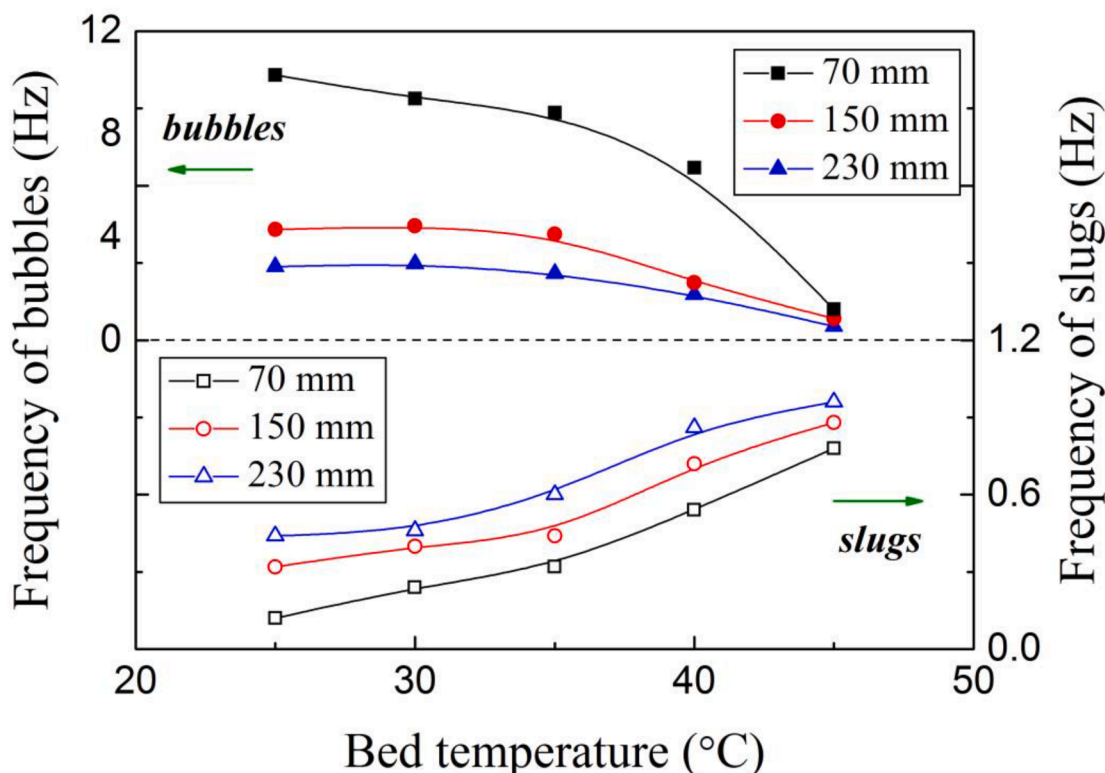


Fig. 9. Frequency of bubbles and slugs at different measurement heights and inter-particle force.

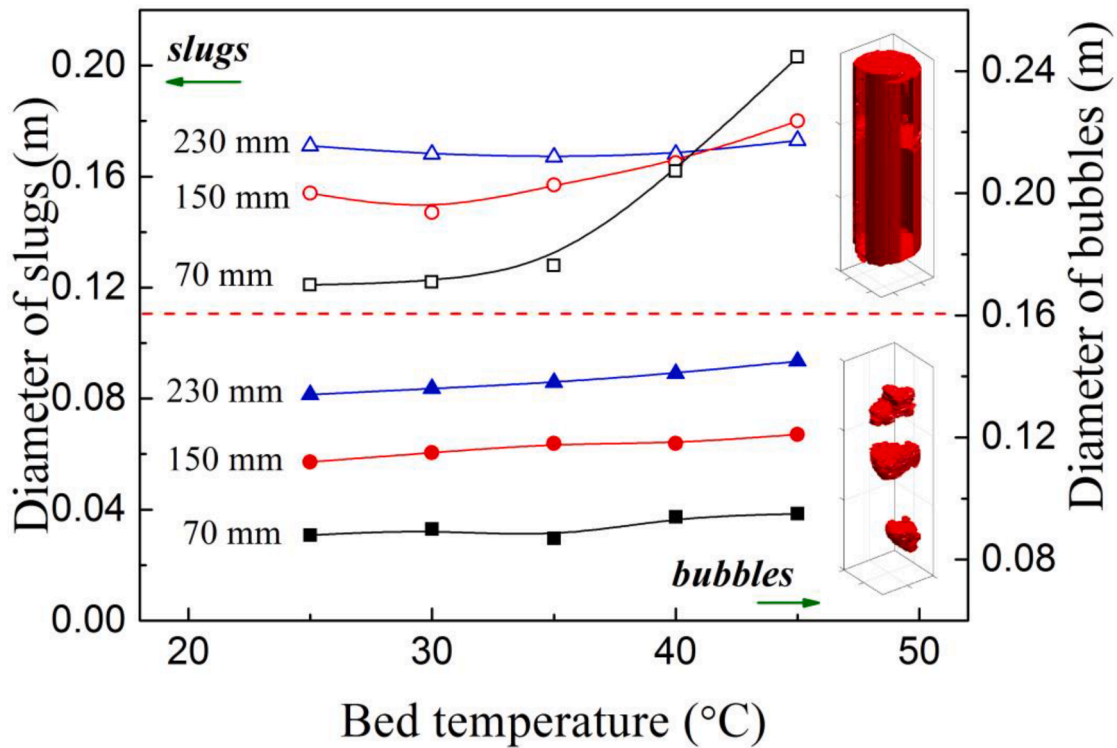


Fig. 10. Equivalent diameter of bubbles and slugs as a function of inter-particle force.

increases (Fig. 11(a)). The distribution at 25 °C agrees with the Gamma fitting curve. As the inter-particle force increases, the distribution becomes narrower and deviates from the fitting curve. Similar trends were also observed for slugs as the temperature increases from 25 °C to 35 °C. The trends imply that the presence of inter-particle force leads to a uniform distribution of bubble and slug sizes. Under the strongest inter-particle force, the distribution of slug size becomes wide and agrees with the Gamma fitting curve. The bed presents an alternative status to whole-bed slugging and bubbling fluidization, allowing for the wide distribution. Therefore, the size of slugs varies over a wider range.

### 3.2.4. Relationship between equivalent diameter and rising velocity

Fig. 12 shows the rising velocity of bubbles and slugs as a function of their equivalent diameter. Fig. 12 also plots the results predicted with the equations from Davidson and Harrison for bubbles and slugs (Davidson and Harrison, 1963; Davidson and Harrison, 1971), as follows.

$$U_b = U_g - U_{mf} + 0.71\sqrt{gD_b} \quad (3)$$

$$U_s = U_g - U_{mf} + 0.35\sqrt{gD} \quad (4)$$

where  $U_b$  and  $U_s$  are the rising velocity of bubbles and slugs,  $U_g$  is the superficial gas velocity,  $U_{mf}$  is the minimum fluidization velocity,  $g$  is the acceleration of gravity,  $D_b$  is the equivalent diameter of bubbles, and  $D$  is the inner diameter of column.

Qualitatively, the rising velocity of bubbles agrees with the theory: the bigger they are, the faster they rise. Quantitatively, the rising velocity of most bubbles falls below their prediction values at a given size. On the one hand, Eq. (3) was developed for isolated bubbles free of the wall effect. The present work was performed in a small column in which bubbles rise along the column wall. The wall effect, therefore, reduces bubble rising velocities (Rüdisüli et al., 2012b). On the other hand, the bubbles rise via the displacement of particles sliding down the bubble walls to the bottom (Davidson and Harrison, 1971). The inter-particle force serves as internal friction acting between adjacent particles. The

friction imposes a resistance to the flow of particles thus reducing the rising velocity of the bubbles.

Near the gas distributor (Fig. 12(b)), the frequency and size of slugs increase with the inter-particle forces because the inter-particle force facilitates the coalescence of bubbles, which easily triggers slugging. Generally, the rising velocity of slugs is independent of their size, which is consistent with the theory. The slugs are involved in whole-bed slugging, which pushes the entire bed upwards. The rising slugs must overcome the friction and cohesive force between the particles and the column wall to continue to rise. Such an effect was not considered in theory because whole-bed slugging does not exist in fluidization without inter-particle force. Therefore, the predicted rising velocity is larger than the measured values. With the increase of the measurement height, the slug rising velocity increases and shows a dependence on their size, especially at the bed surface (Fig. 12(f)). Higher rising velocity was observed for larger slugs. This is analogous to the behavior of bubbles rather than slugs. The abnormal behavior is attributed to various slugging patterns arising at different measurement heights and inter-particle force.

### 3.3. Slugging pattern

Three types of “slug flow” arises with an increase in the inter-particle force, name type A-C, as represented in Fig. 13. **Type A:** The slugs come from the bubbles with dimensions approaching the column diameter. Particles rain down on either side of the slug allowing its upward motion. This type of slug flow is likely to occur in a fluidized bed operating with a high gas velocity. The rising velocity of type A slug flows is higher than the other two types. **Type B:** As the slug grows and occupies the entire cross-section, the bed presents a successive dense and dilute region. The gas passes through the dense particulate region, and the particles rain down uniformly. This type is common in small columns where bubbles are large relative to the bed diameter. Since the presence of inter-particle force enlarges the bubbles in the bed, type B is also common in the present work. The rising of the slugs must overcome the friction between the particles and the bed wall, as the wall effect

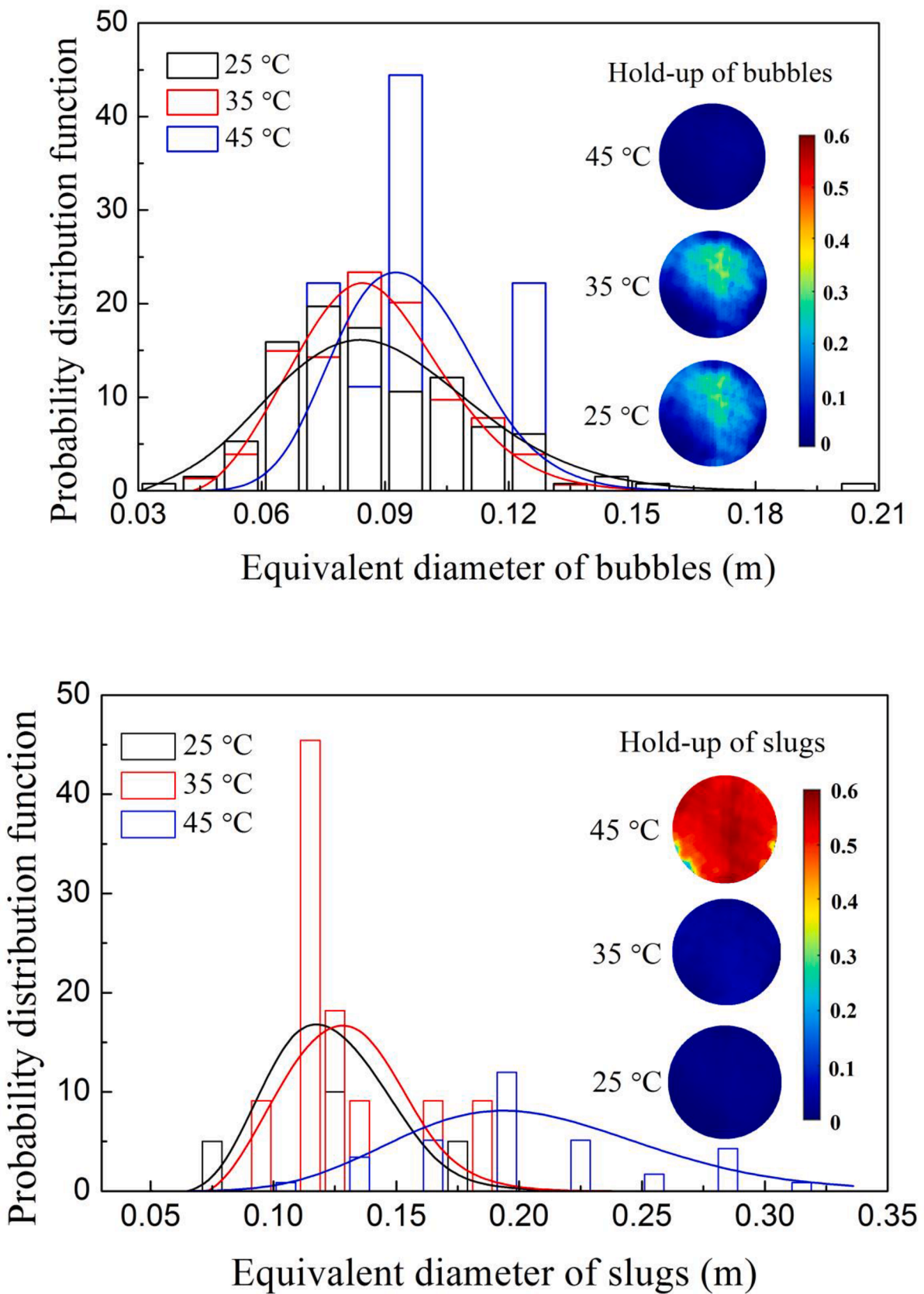


Fig. 11. Effects of inter-particle force on size distribution of bubbles and slugs in the vicinity of gas distributor.

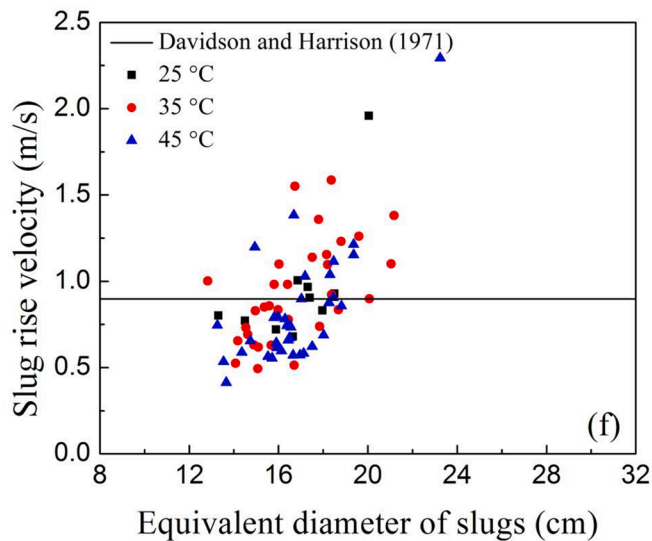
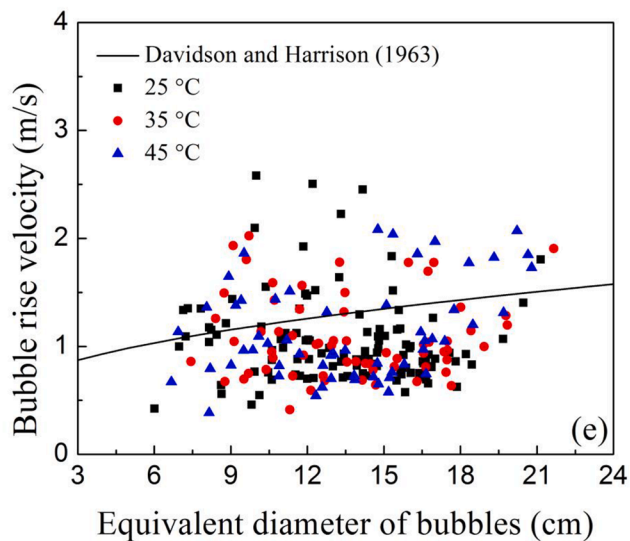
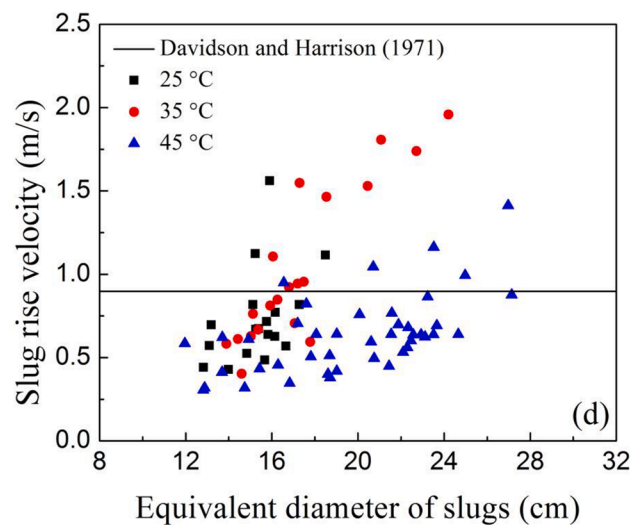
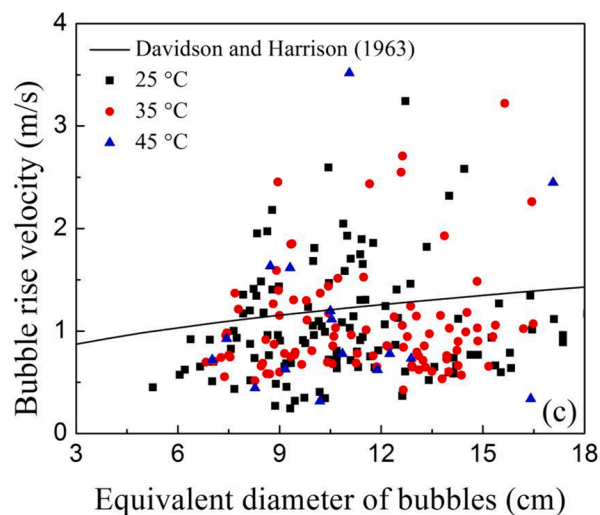
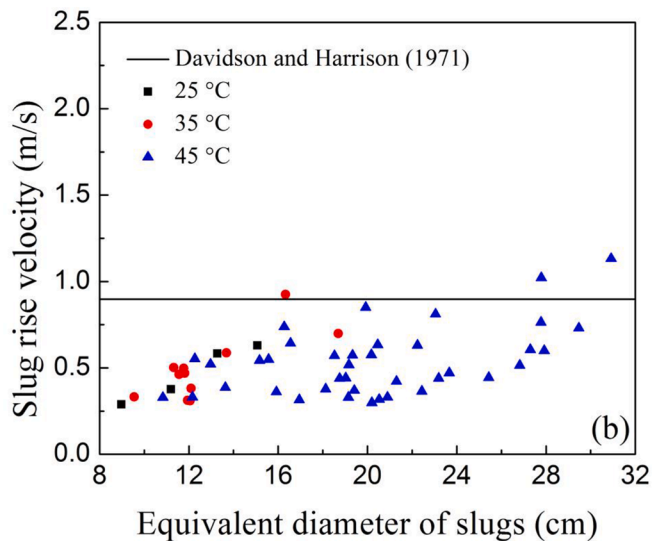
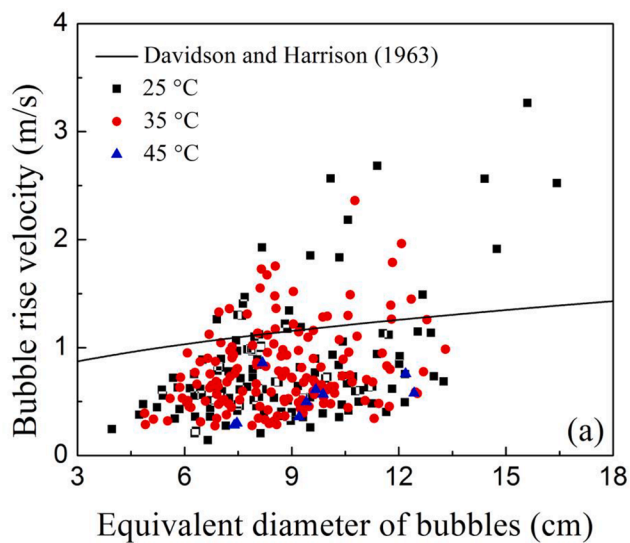


Fig. 12. Relationship between rising velocity and equivalent diameter of bubbles and slugs. Bubbles: (a) 70 mm, (c) 150 mm, (e) 230 mm. Slugs: (b) 70 mm, (d) 150 mm, (f) 230 mm.

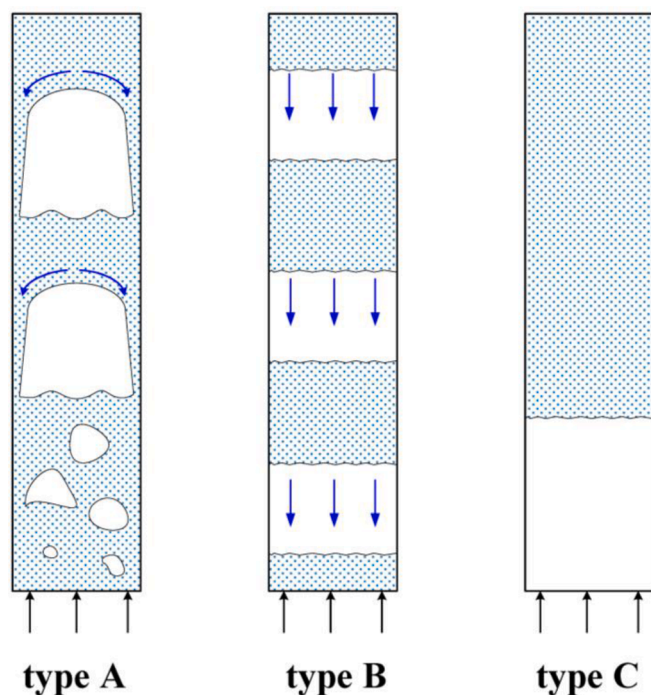


Fig. 13. Schematic of slugging patterns during fluidization with inter-particle force.

controls the slug motion. Therefore, this slug flow's rising velocity is lower than type A. **Type C**: When the inter-particle force is strong enough, the slug grows by capturing other free particles. Finally, the entire bed rises. The bed structure is so compact that few gases can percolate through the particulate phase. The friction and cohesive force between the column wall and the entire bed imposes a strong resistance for slug rising. Therefore, the rising velocity of type C slug flow is the lowest of the three types. Type C is a unique characteristic for a bed with a strong inter-particle force.

Recalling Fig. 12, most slugs detected at 230 mm belong to type A or B, as they are large and rise fast. The slug flow of type C ends with the rupture of particle slug during rising, and is challenging to detect at higher heights. Therefore, the slugs of type C detected near the bed surface are small and rise slowly. All of these slugging patterns present near the bed surface, therefore the slug rising velocity is found to vary with slug size.

#### 4. Concluding remarks

This work employed X-ray tomography to capture the “voids” in a bubbling column with inter-particle forces, and distinguished them as bubbles and slugs. The properties of bubbles and slugs were extracted, including the cross-sectional hold-up, frequency, average equivalent diameter, and size distribution. Void dependence on measurement heights and inter-particle force were also analyzed. The following conclusions may be drawn from the experimental results:

- (1) **Bubbles**: The gas-holding capacity of the emulsion phase is enhanced when the inter-particle force increases to a certain extent. This leads to a decline in bubble frequency and a gentle increase in bubble diameter. At the same time, bubble size distribution becomes narrower. Bubbles rise slower than what is theoretically predicted due to the wall effect and resistance from inter-particle force.
- (2) **Slugs**: The frequency and diameter of slugs increase with inter-particle force. Under a mild force, the slug diameter increases with the measurement height due to large bubbles that induce

slugging. When the inter-particle force is strong enough, the slug diameter decreases with the measurement height because the slugs in whole-bed slugging may rupture in the rising process. Near the gas distributor, the slug rising velocities are independent of their sizes. By contrast, a higher velocity is seen for large-sized slugs due to different slugging patterns near the bed surface.

- (3) **Slugging pattern**: Three types of slug flow arise with an increase in the inter-particle force. The slug flows of Type A come from large bubbles, allowing the raining down of particles from the side. Type B presents a successive dense and dilute region where the wall effect controls the slug motion. Type C is the whole-bed slugging in which the entire bed rises. Both type B and C can be regarded as breakdown of fluidization.

#### CRedit authorship contribution statement

**Jiliang Ma**: Conceptualization, Writing – original draft, Writing – review & editing, Funding acquisition. **Daoyin Liu**: Software, Resources. **Xiaoping Chen**: Writing – review & editing. **Cai Liang**: Writing – review & editing. **J. Ruud van Ommen**: Data curation, Supervision.

#### Declaration of Competing Interest

The authors declare that they have no known competing financial interests or personal relationships that could have appeared to influence the work reported in this paper.

#### Acknowledgements

This work is supported by the National Natural Science Foundation of China (51806036) and the Natural Science Foundation of Jiangsu Province (BK20180398). We would like to thank Mr. Evert C. Wagner and Prof. Robert F. Mudde for valuable suggestions during the experiment.

#### References

- Azizpour, H., Sotudeh-Gharebagh, R., Mostoufi, N., Zarghami, R., 2012. Characterization of regime transition in fluidized beds at high velocities by analysis of vibration signals. *Ind. Eng. Chem. Res.* 51, 2855–2863. <https://doi.org/10.1021/ie200863y>.
- Bartels, M., Lin, W., Nijenhuis, J., Kapteijn, F., van Ommen, J.R., 2008. Agglomeration in fluidized beds at high temperatures: mechanisms, detection and prevention. *Prog. Energy Combust. Sci.* 34, 633–666. <https://doi.org/10.1016/j.pecs.2008.04.002>.
- Bouffard, J., Bertrand, F., Chaouki, J., 2012. Control of particle cohesion with a polymer coating and temperature adjustment. *AIChE J* 58, 3685–3696. <https://doi.org/10.1002/aic.13765>.
- Boyce, C.M., Ozel, A., Kolehmainen, J., Sundaresan, S., McKnight, C.A., Wormsbecker, M., 2017. Growth and breakup of a wet agglomerate in a dry gas-solid fluidized bed. *AIChE J* 63, 2520–2527. <https://doi.org/10.1002/aic.15761>.
- Brouwer, G.C., Wagner, E.C., van Ommen, J.R., Mudde, R.F., 2012. Effects of pressure and fines content on bubble diameter in a fluidized bed studied using fast X-ray tomography. *Chem. Eng. J.* 207–208, 711–717. <https://doi.org/10.1016/j.cej.2012.07.040>.
- Davidson, J.F., Harrison, D., 1963. *Fluidized Particles*. Cambridge University Press, Cambridge.
- Davidson, J.F., Harrison, D., 1971. Pilot plant and laboratory scale fluidized reactors at high gas velocities: the relevance of slug flow. In: Davidson, J.F., Harrison, D. (Eds.), *Fluidization*. Academic Press, London, p. 193.
- Escudero, D., Heindel, T.J., 2013. Minimum fluidization velocity in a 3D fluidized bed modified with an acoustic field. *Chem. Eng. J.* 231, 68–75. <https://doi.org/10.1016/j.cej.2013.07.011>.
- Gomez-Hernandez, J., Serrano, D., Soria-Verdugo, A., Sanchez-Delgado, S., 2016. Agglomeration detection by pressure fluctuation analysis during *Cynara cardunculus* L. gasification in a fluidized bed. *Chem. Eng. J.* 284, 640–649. <https://doi.org/10.1016/j.cej.2015.09.044>.
- Kohler, A., Pallares, D., Johnsson, F., 2020. Modeling axial mixing of fuel particles in the dense region of a fluidized bed. *Energy Fuels* 34, 3294–3304. <https://doi.org/10.1021/acs.energyfuels.9b04194>.
- LaMarche, C.Q., Liu, P., Kellogg, K.M., Hrenya, C.M., 2017. Fluidized-bed measurements of carefully-characterized, mildly cohesive (Group A) particles. *Chem. Eng. J.* 310, 259–271. <https://doi.org/10.1016/j.cej.2016.10.119>.
- Lau, Y.M., Hampel, U., Schubert, M., 2018. Ultrafast X-ray tomographic imaging of multiphase flow in bubble columns – Part 1: Image processing and reconstruction comparison. *Int. J. Multiphase Flow* 104, 258–271. <https://doi.org/10.1016/j.ijmultiphaseflow.2018.02.010>.

- Lin, W., Wang, K., Yang, Y., Huang, Z., Sun, J., Wang, J., Yang, Y., 2020. Characterization of flow pattern of cohesive particles in gas-solid fluidized bed via axial distribution of particle motions. *Int. J. Multiphase Flow* 130, 103355. <https://doi.org/10.1016/j.ijmultiphaseflow.2020.103355>.
- Liu, P., Kellogg, K.M., LaMarche, C.Q., Hrenya, C.M., 2017. Dynamics of singlet-doublet collisions of cohesive particles. *Chem. Eng. J.* 324, 380–391. <https://doi.org/10.1016/j.cej.2017.04.118>.
- Ma, J., Liu, D., Chen, X., 2016. Bubble behaviors of large cohesive particles in a 2D fluidized bed. *Ind. Eng. Chem. Res.* 55, 624–634. <https://doi.org/10.1021/acs.iecr.5b02789>.
- Ma, J., van Ommen, J.R., Liu, D., Mudde, R.F., Chen, X., Wagner, E.C., Liang, C., 2019a. Fluidization dynamics of cohesive Geldart B particles. Part I: X-ray tomography analysis. *Chem. Eng. J.* 359, 1024–1034. <https://doi.org/10.1016/j.cej.2018.11.082>.
- Makkawi, Y.T., Wright, P.C., 2004. Tomographic analysis of dry and semi-wet bed fluidization: the effect of small liquid loading and particle size on the bubbling behavior. *Chem. Eng. Sci.* 59, 201–213. <https://doi.org/10.1016/j.ces.2003.09.030>.
- Maurer, S., Wagner, E.C., Schildhauer, T.J., van Ommen, J.R., Biollaz, S.M.A., Mudde, R.F., 2015a. X-ray measurements of bubble hold-up in fluidized beds with and without vertical internals. *Int. J. Multiphase Flow* 74, 118–124. <https://doi.org/10.1016/j.ijmultiphaseflow.2015.03.009>.
- Maurer, S., Wagner, E.C., van Ommen, J.R., Schildhauer, T.J., Teske, S.L., Biollaz, S.M.A., Wokaun, A., Mudde, R.F., 2015b. Influence of vertical internals on a bubbling fluidized bed characterized by X-ray tomography. *Int. J. Multiphase Flow* 75, 237–249. <https://doi.org/10.1016/j.ijmultiphaseflow.2015.06.001>.
- McLaughlin, L.J., Rhodes, M.J., 2001. Prediction of fluidized bed behaviour in the presence of liquid bridges. *Powder Technol* 114, 213–223. [https://doi.org/10.1016/S0032-5910\(00\)00325-9](https://doi.org/10.1016/S0032-5910(00)00325-9).
- Mudde, R.F., 2011. Bubbles in a fluidized bed: a fast X-ray scanner. *AIChE J* 57, 2684–2690. <https://doi.org/10.1002/aic.12469>.
- Mudde, R.F., 2010. Double X-ray tomography of a bubbling fluidized bed. *Ind. Eng. Chem. Res.* 49, 5061–5065. <https://doi.org/10.1021/ie901537z>.
- Parveen, F., Briens, C., Berruti, F., McMillan, J., 2013. Effect of particle size, liquid content and location on the stability of agglomerates in a fluidized bed. *Powder Technol* 237, 376–385. <https://doi.org/10.1016/j.powtec.2012.12.021>.
- Rüdisüli, M., Schildhauer, T.J., Biollaz, S.M.A., van Ommen, J.R., 2012a. Monte Carlo simulation of the bubble size distribution in a fluidized bed with intrusive probes. *Int. J. Multiphase Flow* 44, 1–14. <https://doi.org/10.1016/j.ijmultiphaseflow.2012.03.009>.
- Rüdisüli, M., Schildhauer, T.J., Biollaz, S.M.A., van Ommen, J.R., 2012b. Bubble characterization in a fluidized bed by means of optical probes. *Int. J. Multiphase Flow* 41, 56–67. <https://doi.org/10.1016/j.ijmultiphaseflow.2012.01.001>.
- Seville, J.P.K., Clift, R., 1984. The effect of thin liquid layers on fluidisation characteristics. *Powder Technol.* 37, 117–129. [https://doi.org/10.1016/0032-5910\(84\)80011-X](https://doi.org/10.1016/0032-5910(84)80011-X).
- Shabaniyan, J., Fotovat, J., Chaouki, J., Bouffad, J., 2013. Fluidization behavior in a gas-solid fluidized bed with thermally induced inter-particle forces. In: *10th International Conference on Circulating Fluidized Beds and Fluidization Technology - CFB-10*, T. Knowlton (PSRI Eds.), ECI Symposium Series. New York, pp. 738–745.
- Shabaniyan, J., Chaouki, J., 2014. Local characterization of a gas-solid fluidized bed in the presence of thermally induced interparticle forces. *Chem. Eng. Sci.* 119, 261–273. <https://doi.org/10.1016/j.ces.2014.08.037>.
- Shabaniyan, J., Chaouki, J., 2017. Effects of temperature, pressure, and interparticle forces on the hydrodynamics of a gas-solid fluidized bed. *Chem. Eng. J.* 313, 580–590. <https://doi.org/10.1016/j.cej.2016.12.061>.
- Shabaniyan, J., Chaouki, J., 2016. Influence of interparticle forces on solids motion in a bubbling gas-solid fluidized bed. *Powder Technol* 299, 98–106. <https://doi.org/10.1016/j.powtec.2016.05.027>.
- Shabaniyan, J., Chaouki, J., 2015. Hydrodynamics of a gas-solid fluidized bed with thermally induced interparticle forces. *Chem. Eng. J.* 259, 135–152. <https://doi.org/10.1016/j.cej.2014.07.117>.
- van der Schaaf, J., Schouten, J.C., Johnsson, F., van den Bleek, C.M., 2002. Non-intrusive determination of bubble and slug length scales in fluidized beds by decomposition of the power spectral density of pressure time series. *Int. J. Mult. Flow* 28, 865–880. [https://doi.org/10.1016/S0301-9322\(01\)00090-8](https://doi.org/10.1016/S0301-9322(01)00090-8).
- Wang, T., He, Y., Tang, T., Peng, W., 2016. Experimental and numerical study on a bubbling fluidized bed with wet particles. *AIChE J* 62, 1970–1985. <https://doi.org/10.1002/aic.15195>.
- Weber, S., Josset, S., Briens, C., Berruti, F., Gray, M., 2011. Predicting agglomerate fragmentation and agglomerate material survival in fluidized beds. *Powder Technol* 210, 87–102. <https://doi.org/10.1016/j.powtec.2011.02.010>.
- Wormsbecker, M., Pugsley, T., 2008. The influence of moisture on the fluidization behaviour of porous pharmaceutical granule. *Chem. Eng. Sci.* 63, 4063–4069. <https://doi.org/10.1016/j.ces.2008.05.023>.
- Xu, H., Zhong, W., Jin, B., Wang, J., 2014. Flow pattern and transition in gas-liquid-solid three phase spouted bed. *Powder Technol* 267, 18–25. <https://doi.org/10.1016/j.powtec.2014.07.010>.
- Xu, H., Zhong, W., Yu, A., Yuan, Z., 2015. Spouting characteristics of wet particles in a conical-cylindrical spouted bed. *Ind. Eng. Chem. Res.* 54, 9894–9902. <https://doi.org/10.1021/acs.iecr.5b02742>.
- Zhou, Y., Shi, Q., Huang, Z., Wang, J., Yang, Y., 2016. Effects of liquid action mechanisms on hydrodynamics in liquid-containing gas-solid fluidized bed reactor. *Chem. Eng. J.* 285, 121–127. <https://doi.org/10.1016/j.cej.2015.09.058>.
- Zhou, Y., Shi, Q., Huang, Z., Wang, J., Yang, Y., 2017. Particle agglomeration and control of gas-solid fluidized bed reactor with liquid bridge and solid bridge coupling actions. *Chem. Eng. J.* 330, 840–851. <https://doi.org/10.1016/j.cej.2017.07.117>.